LAWRENCE
LIVERMORE
NATIONAL
LABORATORY

UCRL-JRNL-230851

Laser heating of solid matter by light pressure-driven shocks

K. Akli, S. B. Hansen, A. J. Kemp, R. R. Freeman, F. N. Beg, D. Clark, S. Chen, D. Hey, K. Highbarger, E. Giraldez, J. Green, G. Gregori, K. Lancaster, T. Ma, A. J. MacKinnon, P. A. Norreys, N. Patel, P. Patel, C. Shearer, R. B Stephens, C. Stoeckl, M. Storm, W. Theobald, L. Van Woerkom, R. Weber, M. H. Key

May 10, 2007

Physical Review Letters

Updated October 14, 2003

Laser heating of solid matter by light pressure-driven shocks

K. U. Akli[1,2], S. B. Hansen[1], A. J. Kemp[1], R. R. Freeman[2,3], F. N. Beg[4], D. C. Clark[3], S. Chen[4], D. Hey [1,2], K. Highbarger [3], E. Giraldez[6], J. Green[5], G. Gregori[5], K. Lancaster[5], T. Ma[4], A. J. MacKinnon[1], P. Norreys[5], N. Patel[3], P. K. Patel[1], C. Shearer[6], R. B. Stephens[6], C. Stoeckl[7], M. Storm[7], W. Theobald[7], L. Van Woerkom[3], R. Weber[3], and M. H. Key[1].

[1]*Lawrence Livermore National Laboratory,*

7000 East Ave, Livermore, CA 94550-9234, USA

[2]*University of California, Davis, Davis, CA 95616, USA*

[3]*The Ohio State University, Columbus, Ohio 43210, USA*

[4]*University of California, San Diego, San Diego, CA 92093, USA*

[5]*Rutherford Appleton Laboratory, Chilton, Didcot, Oxon, OX11 0QX, UK*

[6]*General Atomics, San Diego, CA 92186, USA and*

[7]*University of Rochester-Laboratory for Laser Energetics, Rochester, NY 14623, USA*

(Dated: May 2, 2007)

Abstract

Heating by irradiation of a solid surface in vacuum with 5×10^{20} Wcm^{-2}, 0.8 ps, 1.05 μm wavelength laser light is studied by x-ray spectroscopy of the K-shell emission from thin layers of Ni, Mo and V. A surface layer is heated to ~ 5 keV with an axial temperature gradient of 0.6 μm scale length. Images of Ni Ly_α show the hot region has a ~ 25 μm diameter, much smaller than ~ 70 μm region of K_α emission. 2D particle-in-cell (PIC) simulations suggest that the surface heating is due to a light pressure driven shock.

PACS numbers:

High-intensity laser matter interaction and energy transport by laser generated MeV electrons are widely investigated, both for novel basic science and for applications which include bright sources of multi-10 keV x-rays for probing high energy density matter [1], production of collimated proton plasma jets at energies up to almost 50 MeV [2, 3], and fast ignition of inertial confined fusion [4]. Understanding absorption of laser radiation at high intensities, the production of MeV electrons, and energy transport with associated isochoric heating is crucial to the development of these applications.

The conversion efficiency of the laser energy to MeV electrons has been measured to reach $>$ 30% at intensities of $\geq 3 \times 10^{19}\ Wcm^{-2}$ [5, 6]. Fast ignition experiments heating a compressed plasma via a hollow cone indicated laser-to-plasma energy coupling efficiency of $\sim$ 20% [7, 8]. The formation of a hot surface layer by sub ps pulsed laser irradiation at intensities $>$ $10^{19}\ Wcm^{-2}$ has been reported by Nishimura et al.(2005) and by Theobald et al.(2006), showing respectively a 0.5 μm thick hot layer at $10^{19}\ Wcm^{-2}$ and a 1.0 μm thick hot layer at $\sim 4 \times 10^{20}\ Wcm^{-2}$. At such high intensities, the collisional range of the hot electrons produced by absorption of the laser radiation is more than two orders of magnitude greater than the thickness of the heated layer and the physics of the heating challenges current understanding.

In this letter, we report a more detailed study of hot surface layer formation at intensities $\sim 5 \times 10^{20}\ Wcm^{-2}$ using K- shell spectroscopy of layered targets, monochromatic imaging of K-shell emission and 2D PIC modeling. The hot surface layer is attributed to heating by a light pressure -driven shock wave.

The experiments used the Vulcan Petawatt laser system at the Rutherford Appleton Laboratory [9]. The laser pulse had a wavelength of 1.054 μm, 0.8 ps duration, 400J energy and a peak intensity of $5 \times 10^{20}\ Wcm^{-2}$. An f/3 off-axis parabola focused the beam to 7 μm diameter at half peak intensity with $\sim$ 30% of the energy in a 15 μm diameter and the remaining energy distributed over wings. The amplified spontaneous emission (ASE) contrast ratio was 10^{-7} in intensity and 10^{-4} in energy. The targets were 400 $\mu m \times 400\ \mu m \times$ 5 μm square foils of Mo with two thin tracer layers: a 0.5 μm thick Ni layer located at the irradiated (front) surface or under various depths of Mo and a 1 μm thick V layer located at the rear surface.

A spherically bent Bragg crystal imager [10, 11] normally used to image Cu K_α (8.05 keV) recorded nominally Ni Ly (8.07 keV) images, taking advantage of the quasi-continuum of

satellites to Ni Ly_α. The crystal imager gave Ni Ly_α images with full width at half maximum $\sim$ 25 μm (Fig.1). This indicates that the highest temperatures are confined radially to less than about ~ 25 μm diameter.

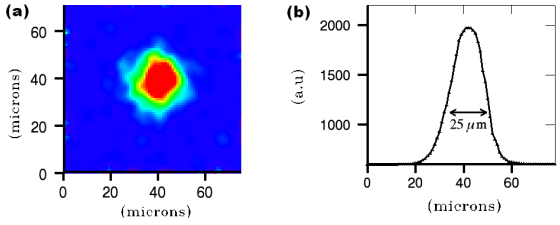

FIG. 1: (a) 2D spatially resolved Ni Ly_α image of a 400 $\mu m \times 400$ $\mu m \times 5$ μm target with a 0.5 μm Mo overlay. (b) Horizontal lineout showing a full width at half maximum of $\sim 25 \mu m$.

Two Highly Ordered Pyrolytic Graphite (HOPG) crystal spectrometers [12] were used to record spectra from the front and back sides of the target. Each HOPG had two channels and each channel had two crystals in close edge contact to increase the spectral range. The front HOPG was angled for the Ni K-shell spectrum; the rear HOPG was optimized for V. The spectra were recorded on an image plate detector [13]. Ni K-shell x-ray spectra were recorded from both the front and rear HOPG instruments for targets with the Ni layer on the surface or buried below Mo layers of 0.5, 1.0 or 2.5 μm thickness. The spectra from Ni at depths up to 1 μm are shown in Fig. 2 (a) with the main emission features from Ni (and Mo in second order) labeled. The Ni Ly_α (8.07 keV) and He_α (7.76 keV) emission lines are intense when the Ni layer is on the target surface, have sharply reduced intensity with any Mo overlay, and are practically eliminated for Mo thicknesses of 1 μm and greater, giving direct experimental evidence that the highest temperatures are in a surface layer < 1 μm thick. The cold K_α (7.48 keV) feature caused by inner-shell ionization of low charge states of Ni is observed for all Ni layer depths. Vanadium spectra showed cold K_α and K_β but no thermal lines, suggesting from spectroscopic modeling that the rear-side temperature of the target was less than 400 eV.

To diagnose the plasma conditions from the Ni spectra, we have used the collisional-radiative model SCRAM [14]. Data from the Flexible Atomic Code (FAC) [15] for neutral to H-like Ni was used to construct a complete and accurate set of levels and rate data based on fine-structure/unresolved transition array (UTA) hybrid level structure [14]. After calculation of collisional rates in an arbitrary electron distribution, SCRAM forms

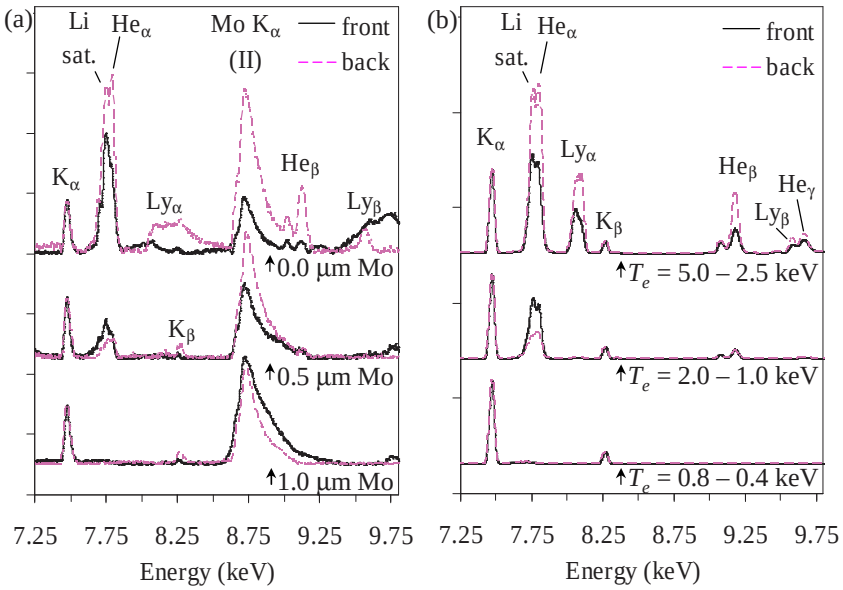

FIG. 2: Color online - (a) Experimental spectra from the front and back sides of 0.5 μm Ni layers buried under various Mo layer depths, normalized to Ni K_α. The broad feature at 8.75 keV is Mo K_α in second order. (b) Modeled spectra of Ni layers at various depths with temperature and density profiles discussed in the text (Mo was not modeled).

configuration-averaged levels for high-lying and multiply-excited states, solves the set of coupled rate equations for level populations, repopulates the averaged states with a better-than-statistical method roughly following the procedure given in Ref. [16], and generates synthetic spectra. Hot electrons were modeled using a Maxwellian distribution whose 1 MeV temperature was estimated from the laser intensity pattern in the focal spot and the pondermotive potential. The collisional-radiative calculations are relatively insensitive to the hot electron temperature [17]. The hot electron fraction $f_{hot} = n_{hot}/n_e$ in the solid target was estimated to be less than 1%, based on an upper limit conversion efficiency of laser light of 50% and a hot electron injection area on the order of 70 m corresponding to the K spot diameter measured on similar thin Cu targets [11]. Although the hot electrons dominate the cold K_α production, their number density is too small to have a significant effect on the ionization balance at solid densities. And since the hot electrons and associated fast ions expand much more rapidly than any high density thermal region, f_{hot} should always be less than 1% during emission of the thermal K-shell spectrum.

To determine the characteristics of the 25 μm heated region, we calculated steady-state synthetic spectra for slices of the target corresponding to 1/5 of the total Ni layer at various temperatures and densities. Within each 0.1 μm slice, the escape factor formalism was used to estimate self-consistent opacity effects and the emissivity (ε) and opacity (κ) along the line of sight of the HOPG were calculated. Using this set of $\varepsilon(T, \rho, \nu)$ and $\kappa(T, \rho, \nu)$, we attempt to find consistent temperature and density profiles that reproduce the major features of the experimental emission spectra after the effects of transport through neighboring Ni layers and instrumental broadening ($E/\Delta E = 200$) were included. The best-fit synthetic spectra, given in Fig. 2 (b), reflect the unambiguous experimental evidence for a thin hot surface layer. The He_α, He_β, Ly_α, and Ly_β emission from the rear HOPG spectrum of the targets with 0.0 and 0.5 μm Mo layers can be simultaneously fit by a hot layer with a maximum temperature of $\sim 5\ keV$ and an e-folding length of about 0.6 μm, giving a temperature which decays rapidly from 5 keV in the first 0.1 μm of the target to 2 keV at a depth of 0.5 μm and finally to less than 600 eV at a depth of 1.3 μm. The Ly_β to He_β lines were favored for this determination because the measured Ly_α line, shown in Fig. 2, was compromised by the joint in the HOPG crystal; more recent measurements without the joint, but with a less complete data set, show a narrower Ly_α feature that more closely resembles the modeled spectra.

If the heated region remained solid, the emission recorded on the rear HOPG would be attenuated along its path through cooler, more opaque material. Normalizing both the front and rear HOPG spectra to the optically thin ($\tau < 0.1$) K_α line, we find that rear HOPG emission is indeed less intense than the front HOPG emission when Ni is buried under 0.5 μm of Mo. But when the Ni is on the target surface, the reverse is seen: the rear HOPG is more intense than the front HOPG. This could be caused by expansion of the target in a blow-off region, since opacities tend to increase with the larger ground state populations found at lower densities. We can fit the He_α emission from both the front and rear HOPG instruments by allowing the target to expand so that the first 0.1 μm of the target has a density of 0.2 g/cc, the second has a density of 1 g/cc, the third a density of 5 g/cc, and the remainder of the target stays at solid density (8.91 g/cc).

In addition to these temperature and density gradients at different target depths, radial temperature gradients are clearly evidenced by the different diameters of the Ly_α-and cold-K_α emission regions (25 μm and 70 μm, respectively). It should be emphasized that

these temperature and density gradients are merely the simplest set of consistent profiles that describe the gross features of the experimental data from all four buried layer depths simultaneously and may be not be unique. In particular, the cooling associated with hydrodynamic expansion could amplify the effect of opacity through the expanded surface layers, thereby decreasing the required expansion. Our diagnostics of the time-integrated data also average over the plasma dynamics. We can say that the bulk of the ionization (if not emission) in the heated region probably occurs at near-solid density during the laser pulse, where equilibration time scales between He-like and H-like Ni are on the order of 0.1 ps, rather than in an expanded region, where equilibration time scales increase rapidly to a few ps at 1 g/cc and ∼100 ps at 0.1 g/cc. Our calculations do suggest that K_α and He_α have similar emission durations, since the instantaneous emission spectra using the experimental values for the heated and bulk emission diameters and our estimate of 50% of the laser energy into hot electrons are in reasonable agreement with the experimental K_α/He_α ratios.

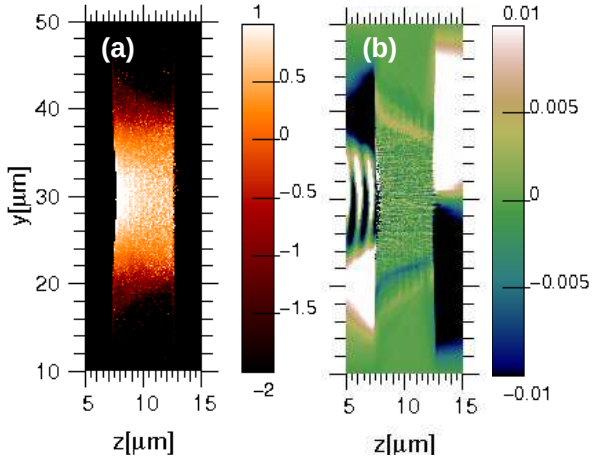

FIG. 3: Result of 2D PIC simulation - (a) electron energy density (arbitrary units) and (b) azimuthal magnetic field in units of B0=2MG at time 100fs

To investigate the physics of the heating process, we have performed numerical simulations with a collisional Particle-in-Cell (PIC) code in two dimensions [18]. The target is modeled as a 5 μm thick slab of solid density Mo^{+5}, resulting in an electron density of roughly $2 \times 10^{23} cm^{-3}$, with periodic boundary conditions in the transverse direction. The simulation box has a total size of 30 $\mu m x 60$ μm at a resolution of 80 cells per μm and 10 ions plus 50 electrons per cell. Ionization and radiation are ignored. The laser pulse

intensity profile is modeled as Gaussian in space (10 μm fwhm) and top-hat in time with a maximum of $5 \times 10^{20} W cm^{-2}$ at a wavelength of 1 μm. Fig. 3 shows two-dimensional aspects of our simulation after 100 fs . The electron energy density $\int (\gamma(p) - 1) m_e c^2 f(p) d^3p$ is plotted in Fig. 3a. Note that most of the energy is confined to the laser spot region, while hot electrons are present throughout most of the target. Strong heating occurs only over the first 0.3 μm. Figure 3b plots the cycle-averaged azimuthal magnetic field. In front of the target there is a standing wave from the laser irradiation, inside the target one can see the filamentary structure of electron transport with strong filamentation near the front surface and a global azimuthal field indicating a net injected current. The azimuthal magnetic fields in front of and behind the target can be ascribed to the fountain effect [19]. Figure 4 shows central line-outs of our 2D simulation. The longitudinal ion phase space shows the signature of a light pressure-driven ion shock [20–22] with a group of ions moving at the flow velocity behind the shock and a smaller group of reflected ions at twice that velocity. The electron number density shows the compression by the shock. On top of that we have plotted a line out of the energy density from the center of Fig.3a. The fact that this quantity increases by more than an order of magnitude in the shock while particle density increases two-fold illustrates that the material is heated and compressed at the same time. The 250kV potential well shown in Fig. 4b is consistent with the shock acceleration of the ions and with the 250 keV electron temperature seen in the electron energy spectrum in Fig.4c.

The energy spectrum has a few percent fraction of the energy with 5 MeV temperature similar to the ponderomotive potential but the 250 keV bulk temperature is evidence of the reduction of hot electron temperature by light pressure induced steepening of the density gradient [23]. In additional 1D PIC simulations we find that any pre-plasma in front of the target can modify the interaction. Sub-solid-density plasma with a scale length of $\leq 2\mu m$ between critical- and solid density can be snowplowed by the main pulse without deteriorating the shock heating effect but larger amounts of plasma significantly inhibit the heating. Larger scale lengths of plasma at sub-critical densities do not affect the heating.

Our PIC modeling gives strong evidence that the heating process at the front surface is through the light pressure-driven electrostatic shock, which arises from a combination of very-high-intensity irradiation and a pulse duration that is sufficient for the shock to sweep up preformed plasma and propagate into the solid target. Failure to sweep up pre-plasma may explain why no strong surface heating has been observed in other work with 100fs pulses

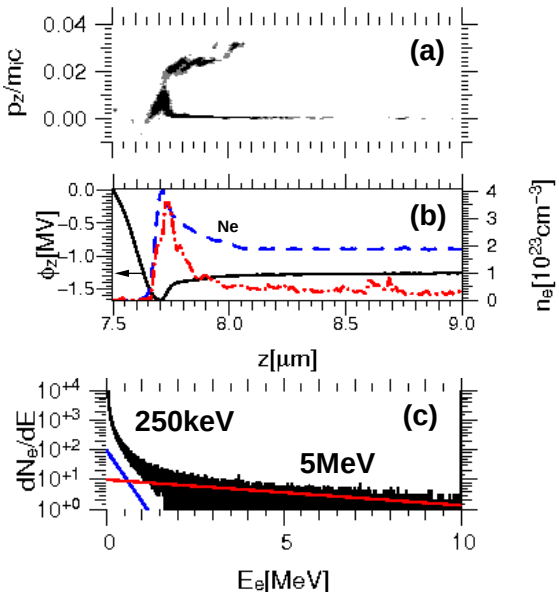

FIG. 4: Result of 2D PIC simulation - (a) longitudinal ion phase space, (b) electric potential (solid), electron density (dashed), and energy density (dash-dotted) along laser irradiation axis ; average over 0.25um ; (c) energy spectrum of all electrons at 100fs.

at intensities similar to ours. Neglect of ionization and radiation in the model means that the 250 keV temperature in the shocked matter is greatly exaggerated but clearly points to strong heating behind the shock. The light pressure at $5 \times 10^{20} W cm^{-2}$ is approximately 170 Gbar giving a shock propagation distance in a 10g/cc solid of 1 μ consistent with the experimentally measured thickness of the hot layer. The light pressure modifies the absorption of the laser pulse, by denting the critical interface [24], and by reducing the average energies of most of the hot electrons far below the ponderomotive potential [23]. Electrons trapped in the electrostatic potential well of the shock add to the shock heating.

The high energy density in the hot layer is of intrinsic interest for high energy density science. The experimentally determined diameter of the hot region size and its thickness suggest that its thermal energy is however about 0.6 J or 0.3% of the laser energy incident on target. It would be a problem for fast ignition if a significant fraction of the energy were trapped at the surface of a solid target but this is not so. An additional $7.5-10\%$ of the laser energy is delivered to the bulk of thin targets by hot electrons that are not confined to the surface layers. This has been confirmed on similar low mass targets using the absolute yield of K-shell fluorescence [11, 25]. Hot electrons also lose a significant fraction of their energy

to ion acceleration in thin targets as evidenced by measurements showing a reduction of the absolute K-shell emission yield with decreasing target thickness [11]. Our thin target data are therefore not inconsistent with earlier estimates of the conversion of 30% conversion to hot electrons at the intensities of this work, which is important for fast ignition.

In conclusion, heating of a sub micron thick layer at near solid density to $\sim 5\ keV$ temperature by $5 \times 10^{20} W cm^{-2}$, 0.8 ps laser irradiation is attributed to the light pressure-driven shock. This is interesting in its own right for creation of high energy density states of matter; but it is not a major drain of electron energy and therefore does not adversely affect fast ignition.

We wish to acknowledge use of the Vulcan laser facility and the PSC code on LLNL's ATLAS computer. Useful discussions with H. Ruhl, Y. Sentoku are acknowledged. This Work was performed under the auspices of the U.S. Department of Energy by the Lawrence Livermore National Laboratory under Contract No. W-7405-ENG-48 with UC.

---

[1] O. L. Landen, D. R. Farley, S. G. Glendinning, and et al., Review of Scientific Instruments **72**, 627 (2001).

[2] A. J. Mackinnon, Phys. Rev. Lett **88**, 215006 (2002).

[3] R. A. Snavely, M. H. Key, S. P. Hatchett, T. E. Cowan, M. Roth, T. W. Phillips, M. A. Stoyer, E. A. Henry, T. C. Sangster, M. S. Singh, et al., Physical Review Letters **85**, 2945 (2000).

[4] M. Tabak, J. Hammer, M. E. Glinsky, W. L. Kruer, S. C. Wilks, J. Woodworth, E. M. Campbell, M. D. Perry, and R. J. Mason, Phys. Plasmas **1**, 1626 (1994).

[5] K. B. Wharton, S. P. Hatchett, S. C. Wilks, M. H. Key, and et al., Physical Review Letters **81**, 822 (1998).

[6] K. Yasuike, M. H. Key, S. P. Hatchett, R. A. Snavely, and K. B. Wharton (2001), vol. 72, p. 1236.

[7] R. Kodama and et al., Nature **412**, 798 (2001).

[8] R. Kodama and et al., Nature **418**, 933 (2002).

[9] C. N. Danson, S. Angood, L. J. Barzanti, and et al., Proc. SPIE **3047**, 505 (1997).

[10] J. A. Koch, Y. Aglitskiy, C. Brown, T. Cowan, R. Freeman, S. Hatchett, G. Holland, M. Key, A. MacKinnon, J. Seely, et al. (2003), vol. 74, pp. 2130–2135.

[11] K. U. Akli, M. H. Key, H. K. Chung, S. B. Hansen, R. R. Freeman, M. H. Chen, G. Gregori, S. Hatchett, D. Hey, N. Izumi, et al., Physics of Plasmas **14**, 023102 (2007).

[12] S. H. Glenzer, G. Gregori, F. J. Rogers, D. H. Froula, S. W. Pollaine, R. S. Wallace, and O. L. Landen, Physics of Plasmas **10**, 2433 (2003).

[13] N. Izumi, R. Snavely, G. Gregori, J. A. Koch, H.-S. Park, and B. A. Remington (2006), vol. 77, p. 10E325.

[14] S. B. Hansen, J. Bauche, c. Bauche-Arnoult, and M. F. Gu, to be published in High Energy Density Physics (2007).

[15] M. F. Gu, Astrophysical Journal **590**, 1131 (2003).

[16] F. B. Rosmej, Europhysics letters **76**, 1081 (2006).

[17] S. B. Hansen and A. S. Shlyaptseva, Physical Review E **70**, 036402 (2004).

[18] H. Ruhl, Plasma Sources Science and Technology **11**, A154 (2002).

[19] J. Denavit, Phys. Rev. Lett. **26**, 1012 (1971).

[20] L. O. Silva, M. Marti, J. R. Davies, and et. al, Physical Review Letters **92**, 015002 (2004).

[21] J. Denavit, Phys. Rev. Lett. **69**, 3052 (1992).

[22] S. Miyamoto and et al., Journal of Plasma and Fusion Research **73**, 343 (1997).

[23] S. C. Wilks, W. L. Kruer, M. Tabak, and A. B. Langdon, Phys. Rev. Lett. **69**, 1383 (1992).

[24] H. Ruhl, in: Introduction to Computational Methods in Many Body Physics, edited by M. Bonitz, Rinton Press (2005).

[25] W. Theobald, K. Akli, R. Clarke, and et al., Phys. Plasmas **13**, 043102 (2006).